International Journal of Microwave and Wireless Technologies, 2016, 8(2), 353–361.
doi:10.1017/S1759078715000100

RESEARCH PAPER

Hybrid MoM–PO analysis of multilayered SIW slot antenna with a dielectric slab radome

REZA BAYDERKHANI[1], KEYVAN FOROORAGHI[1], EMILIO ARNIERI[2] AND BIJAN ABBASI-ARAND[1]

A fast and efficient full-wave hybrid method for the analysis of a multilayered substrate integrated waveguide (SIW) based slot antenna/array radiating into a dielectric slab radome is presented. The antenna structure is modeled as a stacked parallel-plate waveguide hosting metallic posts and coupling and/or radiating slots. To account the radome effects on the SIW antenna, the physical optics method in conjunction with three-dimensional ray trace technique are used to analyze a dielectric slab radome staked on the aperture of the antenna. The field in the SIW structure is expressed by using an expansion in terms of vectorial cylindrical eigenfunctions. Enforcing the boundary conditions on posts yield the scattering amplitude, while slots are modeled as unknown magnetic currents which are found by solving the integral equation derived from the continuity of the field on the slot surface. A double-layered SIW cavity backed slot antenna radiating into a dielectric slab radome is analyzed, and the results compared with high frequency simulation software (HFSS) simulations. It will be shown that the proposed method is fast and efficient and gives results in very good agreement with the most common simulation tools.

Keywords: EM field theory and numerical techniques, Antennas and propagation for wireless systems

Received 31 October 2014; Revised 30 December 2014; Accepted 11 January 2015; first published online 25 March 2015

I. INTRODUCTION

Low cost, low profile and ease of fabrication using standard procedures, such as the printed-circuit-board (PCB) techniques, along with easy integration with other planar circuits are making the substrate integrated waveguide (SIW) technology a promising candidate for microwave and millimeter-wave applications. Firstly as proposed in [1], the SIW technology has been applied to design numerous structures, including power dividers/combiners [2], directional couplers [3], oscillators [4], power amplifier [5], slot array antennas [6], and etc. One of the most popular classes of the SIW-based antennas is slot antennas/arrays [6, 7]. Over the years, SIW slot antennas along with other SIW-based components have been designed and analyzed using approximate analytical methods based on transmission-line theory [8], the equivalent-waveguide-width model [9], two-dimensional, multi-port methods [10] or finite-element (FEM), and finite-difference (FD) based commercial full wave solvers. The former approach has been computationally efficient, but it does not guarantee the accuracy of the final design results. The latter approach can be time consuming and memory demanding for large structures. However, to investigate a general substrate integrated waveguide antenna, an efficient full-wave analysis is required. For these reasons, the general, efficient, and fast analysis of SIW devices and antennas becomes a new challenge that is the object of intense research in the last few years. A rigorous and efficient full-wave analysis of non-radiating SIW devices based on the dyadic Green's function technique is firstly introduced in [11, 12]. The same approach was extended to efficiently analyze the large single-layer [13]/multilayer [14] SIW-based slot antenna array with the beam forming network. However, the design and analysis of the SIW-based slot antennas/arrays, considering the radome effects has not been considered.

In practice, to protect the antenna from a variety of environmental effects, a dielectric radome is always covered in front of the antenna. The presence of a radome can affect the gain, beam width, side lobe level and direction of boresight as well as change the voltage standing wave ratio (VSWR) and input impedance of the antenna. These effects in higher frequencies are more critical. Thus, the ability to accurately predict the effect of a radome on the operation of an antenna in the design process is more desirable. There are many instances in literature discussing the methods for analyzing the dielectric radomes using various numerical approaches [15–18]. However, it seems that in all the above analysis done on the modeling of radomes, the forward decoupling between the antenna and radome was assumed, but a drawback of this decoupling is that reverse coupling from the radome to the antenna was ignored. On the other hand, all the

[1]Tarbiat Modares University, Faculty of Electrical and Computer Engineering, Jalale-Ale- Ahmad Highway, Tehran, Iran. Phone: +98 21 8288 3365
[2]Department of Informatics, Modeling, Electronic and System Engineering (DIMES), University of Calabria, Rende, CS, Italy
Corresponding author:
K. Forooraghi
Email: keyvan_f@modares.ac.ir

aforementioned methods only focus on the analysis of the radomes and the effects of radome on the VSWR but aperture distribution of the antennas are not considered.

Motivated by the aforementioned issues, in this paper a fast and efficient full-wave analysis of a double-layered SIW-based slot antenna/array radiating into a dielectric slab radome is introduced. The approach of [13] has been extended to analyze a double-layered SIW slot antenna/array with arbitrary number of radiating and/or coupling slots. In addition, to account the effects of radome on the SIW antenna, the dielectric slab is analyzed using Ray/PO technique. Finally, the equations with the unknowns are solved to obtain the equivalent surface currents on the aperture of slots. To validate the proposed method, the aforementioned theory is applied to a double layered SIW-based cavity backed slot antenna, that was recently proposed in [7], radiating into a thick dielectric slab radome. A comparison between proposed method results and finite element simulations are presented and discussed. The results show that the proposed method is both accurate and efficient.

II. OVERVIEW OF THE HYBRID METHOD

As noted in the introduction, the proposed hybrid method combines the method of moment (MoM) and Ray/physical optics (PO) technique to analyze the double-layered SIW-based slot antenna radiating into a dielectric stacked radome. (The extension of the formulation to the multilayered case is straightforward and will not be explicated here.) In the proposed hybrid method, the domain of solution is divided into two parts: the high frequency part placed away from the antenna (PO region) including a dielectric stacked radome and low frequency part (MoM region) including a double-layered SIW-based slot antenna (see Fig. 1).

The MoM along with mode matching technique is used to treat the double-layered SIW-based slot antenna (internal region). This is done by representing the field in the post walled structure through the dyadic Green's function of the parallel plate waveguide [11]. Additionally, to analyze the external region, the PO method is employed in conjunction with ray principles to model the field transmission and reflection through the stacked radome's wall. To do so, the equivalence principle is applied on the radome's surface and the forward as well as backward radiation is calculated. The total field in the external region is then obtained by the summation of incident fields impinging from the antenna and scattered fields from the radome. Then the surface integration equation is established on the aperture of slots. Finally, the equations with the unknowns are solved to obtain the equivalent surface currents on the aperture of slots. Consequently, the number of unknowns is given by the number of modes assumed in each slot (Np) multiplied by the number of slots (NS) i.e. $N_p \times N_s$. As a result, the computational efficiency is achieved along with reasonable accuracy using the proposed hybrid method. It should be noted that in spite of pervious researches done for modeling the dielectric radomes, in the application of surface equivalence principle, the effects of back radiation on the antenna aperture distribution and input impedance of the antenna are also accounted. This hybridization of the two techniques is described in detail in Section III.

Given the above presuppositions, the implementation of the proposed hybrid method is as follows:

(1) First the problem is divided into two equivalent sub-problems, (i) MoM region and (ii) PO region.
(2) In MoM region: invoking the field-equivalence principle, the slots are replaced by a metal plate with the equivalent magnetic currents $Minner = M$ and $Mouter = -M$ located onto their respective surfaces.
(3) The unknown magnetic currents M is discretized as a sum of suitable basis functions.
(4) In the PO region: the antenna fields are computed on the radome's surface for each mode of basis function of the radiating slots. These fields are then used as the excitation for the PO treatment of the radome.
(5) PO currents are computed on the inner and outer side of radome's wall. The PO currents are then used as the external source radiating into the free space and antenna aperture.
(6) Invoking the pre-computed PO currents as excitation, a MoM system is generated to find the MoM equivalent currents on the aperture of slots.
(7) The MoM matrix is finally solved and the equivalent currents are determined.

The above steps are discussed below in more detail.

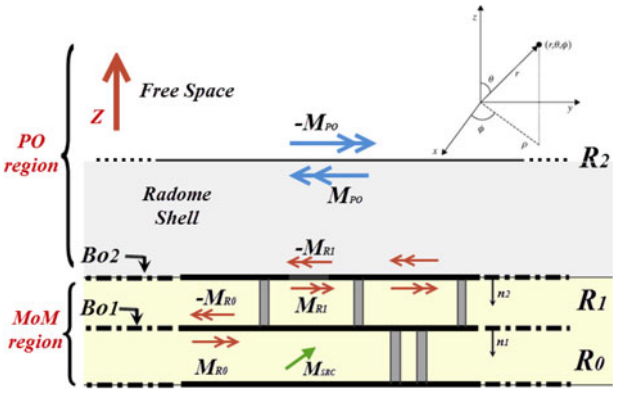

Fig. 1. Stacked-PPW geometry analyzed. A radome shell is located on the top wall of the antenna.

III. PROBLEM FORMULATION

Invoking the surface equivalence principle the original problem is divided into the simpler sub-problems: (i) in MoM region: the slots are short-circuited and the equivalent magnetic currents $Minner = M$ and $Mouter = -M$ are introduced onto their respective surfaces: (ii) in PO region: the equivalent magnetic currents are located on the radome's surface as shown in Fig. 1.

There are two sets of current to consider. The first set is the currents in the MoM region on the aperture of slots. The second set refers to the currents in the PO region on the surface of the radome. To avoid ambiguity the subscripts MM and PO are used to denote the MoM region and the PO region, respectively. In the next sub-sections the detailed analysis of the MoM–PO approach will be discussed.

https://doi.org/10.1017/S1759078715000100 Published online by Cambridge University Press

A) PO region modeling

The PO method is a high frequency technique and appropriate for analyzing the electrically smooth-radii radome efficiently, where the assumption of locally flat surface can be invoked. The PO calculates the surface currents induced on metallic or dielectric surfaces due to an incident electromagnetic field [19]. Thus, in our formulation, the PO method is exploited to analyze the flat dielectric radome, where due to the flatness of the radome surface, the assumption of locally flat surface is satisfied. Based on PO, the equivalent magnetic currents are expressed as the total fields on the internal and external radome surfaces. Thus, the equivalent magnetic current induced on inner and outer surface of radome for qth modes of the jth radiating slot is obtained by

$$M^{PO}_{inner,q,j} = (\widehat{E}^{i}_{q,j} + \widehat{E}^{r}_{q,j}) \times \widehat{n}_1, \tag{1}$$

$$M^{PO}_{outer,q,j} = (\widehat{E}^{t}_{q,j}) \times \widehat{n}_2, \tag{2}$$

where $\widehat{n}_1$ and $\widehat{n}_2$ are the unit normals depicted in Fig. 1. It should be noted that, in our case $\widehat{n}_1 = -\widehat{n}_2$; Also, $\widehat{E}^{i}$, $\widehat{E}^{r}$ and $\widehat{E}^{t}$ refer to the incident, reflected and transmitted fields, respectively. The incident field, $\widehat{E}^{i}_{q,j}$, is radiated by qth modes of the jth radiating (not coupling) slots and evaluated in the inner surface of radome. The reflected fields $\widehat{E}^{r}_{q,j}$ as well as transmitted ones $\widehat{E}^{t}_{q,j}$ are evaluated using ray optics principle. They are given by:

$$\begin{aligned} \widehat{E}_r &= (\widehat{E}_i.\widehat{v}^{i}_{\perp})R_{\perp}\widehat{v}^{r}_{\perp} + (\widehat{E}_i.\widehat{v}^{i}_{||})R_{||}\widehat{v}^{r}_{||}, \\ \widehat{E}_t &= (\widehat{E}_i.\widehat{v}^{i}_{\perp})T_{\perp}\widehat{v}^{t}_{\perp} + (\widehat{E}_i.\widehat{v}^{i}_{||})T_{||}\widehat{v}^{t}_{||}, \end{aligned} \tag{3}$$

where

$$\widehat{v}_{\perp} = \frac{-\widehat{k}_i \times \widehat{n}_1}{|\widehat{k}_i \times \widehat{n}_1|}, \tag{4}$$

$$\begin{aligned} \widehat{v}^{i}_{||} &= \widehat{v}_{\perp} \times \widehat{k}_i, \\ \widehat{v}^{r}_{||} &= \widehat{v}_{\perp} \times \widehat{k}_r, \\ \widehat{v}^{t}_{||} &= \widehat{v}_{\perp} \times \widehat{k}_t, \end{aligned} \tag{5}$$

$\widehat{k}_i$ is the propagation direction of the incident wave and

$$\begin{aligned} \widehat{k}_r &= -\cos(2\theta_i)\widehat{k}_i + \cos(\theta_i)\widehat{n}_1, \\ \widehat{k}_t &= \cos(\theta_i - \theta_t)\widehat{k}_i - \cos(\theta_t)\widehat{n}_1, \\ \cos(\theta_i) &= \widehat{n}_1.\widehat{k}_{,i} \end{aligned} \tag{6}$$

where θ_t is the angle of refraction and can be determined by Snell's law. $R_{\perp}$, $R_{||}$, $T_{\perp}$ and $T_{||}$ are the reflection and transmission coefficients for the perpendicular and parallel polarization and are given by [20]

$$\begin{aligned} R_{\perp} &= \frac{Z_o\cos\theta_i - Z_d\cos\theta_t}{Z_o\cos\theta_i + Z_d\cos\theta_t}, & R_{||} &= \frac{Z_d\cos\theta_i - Z_o\cos\theta_t}{Z_d\cos\theta_i + Z_o\cos\theta_t}, \\ T_{\perp} &= \frac{2Z_o\cos\theta_i}{Z_o\cos\theta_i + Z_d\cos\theta_t}, & T_{||} &= \frac{2Z_d\cos\theta_i}{Z_d\cos\theta_i + Z_o\cos\theta_t}, \end{aligned} \tag{7}$$

where $\boldsymbol{Z}_o$ is the characteristic impedance of the free space and $Z_d = Z_o/\sqrt{\varepsilon_r}$ is the characteristic impedance of the dielectric radome.

As mentioned earlier in Section II, these known PO currents are used as the external sources and affect the antenna field distribution as well as input admittance. These PO currents are next introduced into the MoM matrix to generate the hybrid MoM–PO method. This hybridization along with how these known PO currents affect the MoM matrix are shown in the next sub-section.

B) MoM region modeling

MoM is used for modeling a double-layered SIW antenna including an arbitrary number of radiating/coupling rectangular slots. This antenna radiates into a grounded thick dielectric slab characterized by ε_d and μ_d. The geometry under consideration is illustrated schematically in Fig. 1. The geometry to be considered here is divided into a three distinct regions: *Ro*, also named as interior region, located at the lowest layer of SIW slot antenna/array and includes a generic SIW circuit with arbitrary number of coupling slots and posts excited through coaxial or waveguide ports; *R1* that is the top layer of SIW slot antenna excited by the coupling slots placed on the rear face and radiated into the external region by the slots etched on the top face; and *R2* that is the external region away from the antenna containing a grounded thick dielectric slab stacked on the top wall of the antenna and characterized by the constitutive parameters ε_d and μ_d. The normal vector $\hat{n}_{i+1}$ points into the region R_i; *Bo2* denotes the boundary surface between *R1* and *R2*; and *Bo1* is the boundary between *Ro* and *R1*. The parallel plates that are forming the SIW structure are assumed to be a perfect-electric conductor with infinitesimal thickness. In addition, the permittivity of dielectric materials is assumed in more general form as a complex value. Only one excitation is assumed in this paper. However, if several feeding ports are present, their effects are superposed.

1) INTEGRAL EQUATION

Using the field-equivalence principle, the slots are replaced by a metal plate and modeled as equivalent magnetic currents M flowing on the inner and -M on the outer surface as shown in Fig. 1. As far as narrow rectangular slots are of interest, it can be assumed that there is only transverse electric fields component across the slots, and the magnetic current is completely directed along the longitudinal direction and its transverse dependence is neglected. Applying the boundary conditions on the aperture of slots requires the tangential electric and magnetic fields to continue. The continuity of magnetic field across the surface S of the slots leads to the following general integral equation for each slot i:

$$\widehat{n} \times H^{inner}_{tot}(r) = \widehat{n} \times H^{outer}_{tot}(r) \tag{8}$$

https://doi.org/10.1017/S1759078715000100 Published online by Cambridge University Press

$$\hat{n} \times \left(H_{inc}^{inner}(r) + \sum_{j}^{Ns} H_{M\_slot,j}^{inner}(r) \right), \\ = \hat{n} \times \left(\begin{matrix} H_{inc}^{outer}(r) + \\ + \sum_{j}^{Ns} H_{M\_slot,j}^{outer}(r) + \sum_{q}^{Nq} \sum_{j}^{Ns} H_{j,q}^{PO}(r) \end{matrix} \right) r \in S, _i \tag{9}$$

in which [13]

$$H_{inc}(r) = -j\omega\varepsilon_0\varepsilon_r \cdot \iiint_{V_{SRC}} \bar{G}_{PPW}(r, r').M_{SRC}(r')dr' + H_S^{M_{SRC}}(r), \tag{10}$$

$$H_{M\_slot,j}(r) = -j\omega\varepsilon_0\varepsilon_r \cdot \iint_{S_j} \bar{G}_{PPW}(r, r').M_j(r')dr' + H_S^{M_j}(r), \tag{11}$$

where r and r' define the observation and source point, respectively, M_j is the equivalent magnetic current source defined on the surface of slot j (S_j), $\bar{G}_{PPW}(r, r')$ is the dyadic Green's function of the parallel plate waveguide when all the slots are short-circuited, H_S^M is the field scattered by the metallic posts due to the current M, both given in Appendix A and B, respectively; $M_{SRC}(r')$ is the current-source distribution defined in volume V_{SRC}; and H_{PO} is the magnetic field precomputed by Ray/PO technique modeling the radome effects and has non-zero value only for outer region.

In the application of the above formulas the correct sign of magnetic currents should be assigned carefully because of the possible presence of magnetic currents on both the upper and the lower plates of each PPWs. Due to the opposite directions of the vectors normal to the different interface, they have different sign in integral equation. The equation (9) is the more general form of integral equation and some quantities of (9) may be zero in various regions. Region Ro includes the excitation ports along with coupling slots. Thus in the equation assigned on boundary *Bo1*, the $H^{PO}(r)$ is zero. However, *R1* contains the coupling and radiating slots without excitation ports. Therefore, on the boundary *Bo2* (see Fig. 1), in the equation (9) the $H_{inc}^{inner}(r)$ is zero but because of the presence of PO currents on the radome's surface, $H^{PO}(r)$ is not null. As mentioned earlier, only one excitation source in Ro is assumed. Therefore, in this paper, the $H_{inc}^{outer}(r)$is zero in all regions.

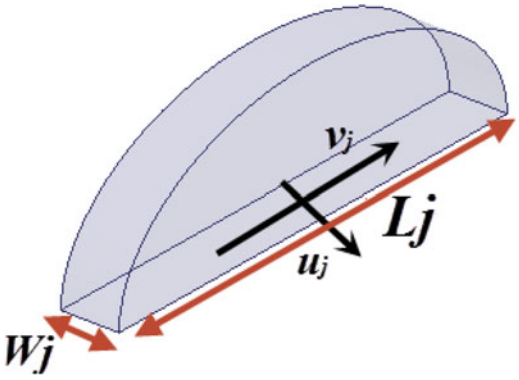

Fig. 2. Shape of basis function.

2) FORMULATION OF HYBRID MOM – PO METHOD

The equivalent magnetic currents which are used to model the slots are expanded in terms of an entire domain sinusoidal basis function, as shown in Fig. 2. The magnetic currents for a slot j are

$$M_j^{MM}(r') = \hat{v}_j \sum_q f_{q,j}(r').V_{q,j} \qquad 1 \le j \le N_s, \tag{12}$$

$$f_{q,j}(r') = \sin\left(k_q(L_j/2 + v_j)\right), \quad |v_j| \le L_j \tag{13}$$

$$k_q = \frac{q\pi}{L_j} \quad \text{and} \quad r' = r_{jq} + u\hat{u}_j + v\hat{v}_j, \tag{14}$$

where r_{jq} is the center of the qth basis function on the slot j, $V_{q,\,j}$ are the unknown expansion coefficients, N_s is the number of slots, L_j is the length of the jth slot and q spans over the number of modes N_q.

Substituting (10)–(14) into the (9) and applying the Galerkin's method, the integral equations can be converted into a system of $N_s \times N_q$ linear equations with $N_s \times N_q$ unknowns

$$h_{p,i} = \sum_{q,j} Y_{q,j}^{p,i}.V_{q,j} \qquad \forall(p, i), \tag{15}$$

where p and q span over the basis functions, while i and j span, the number of slots, *NS*.

$$h_{p,i} = \begin{cases} \iint_{S_i} f_{p,i}\hat{v}_i.H_{inc}(r)\mathrm{d}r & \text{for interior region} \\ 0 & \text{other regions} \end{cases}, \tag{16}$$

$$Y_{q,j}^{p,i} = Y_{q,j}^{p,i}(\text{int1}) + Y_{q,j}^{p,i}(\text{int2}) + Y_{q,j}^{p,i}(ext), \tag{17}$$

$$Y_{q,j}^{p,i}(\text{ext}) = \begin{cases} j\omega\varepsilon_0\varepsilon_d \iint_{S_i} dr \iint_{S_j} dr' f_{p,i}\hat{v}_i.\bar{G}_{ext}(r, r').\hat{v}_j f_{q,j} + \iint_{S_i} dr f_{p,i}\hat{v}_i.H^{PO}(r) \\ 0 \\ \text{for radiating slots} \\ \text{otherwise} \end{cases}, \tag{18}$$

https://doi.org/10.1017/S1759078715000100 Published online by Cambridge University Press

$$Y_{q,j}^{p,i}(\text{int}) = j\omega\varepsilon_o\varepsilon_r.$$
$$\iint_{S_i} dr \iint_{S_j} dr' f_{p,i}\hat{v}_i.\bar{G}_{PPW}(r, r').\hat{v}_j f_{q,j} + \iint_{S_i} dr f_{p,i}\hat{v}_i.H_S^{f_{q,j}}(r), \quad (19)$$

where $Y_{q,j}^{p,i}(\text{int1})$ and $Y_{q,j}^{p,i}(\text{int2})$ are the admittance elements in *Ro* and *R1* regions, respectively and have the same form of (19). In the application of (15) it should be noted that in each region, only corresponding slots should be considered, for example in *Ro* the radiating slots are vanished. The incident field $H_{\text{inc}}(r)$ is defined as the magnetic field radiating into the structure by a port source with short circuited slot. In the above formulation only one port source which is radiated in interior region is assumed. As mentioned before, if several feeding ports are presented, their effects are superposed. The modeling of coaxial as well as waveguide ports radiated in non-radiating SIW structures are explained in [11], but in this paper for the sake of brevity only the coaxial port is assumed. As is well documented in literature, a coaxial probe with inner radius of a and outer radius of b, is modeled as a ring of magnetic current given by [19]

$$M_{SRC}(r') = -\hat{\phi}\frac{V}{|\rho' - \rho_s|\ln(b/a)}\delta(z'), \quad (20)$$

where V is the voltage between the inner and outer conductors, ρ_s is the position of the center of the inner conductor and ρ' is a point inside the annular region where the magnetic current is flowing. As shown previously in [11], by substituting (20) into the (10), the following expression (21) is obtained.

$$H_{inc}(r) = -\frac{2\pi V}{\ln\left(\frac{b}{a}\right)}\frac{\omega\varepsilon}{2h}\sum_m\left(1-\frac{\delta_{mo}}{2}\right)\frac{1}{k_{\rho m}^2}(\nabla\times\hat{z})\cos(k_{zm}z)$$
$$\left\{\begin{array}{l} H_o^{(2)}(k_{\rho m}\rho)\left[J_o(k_{\rho m}\rho) - J_o(k_{\rho m}a)\right] \\ +J_o(k_{\rho m}\rho)\left[H_o^{(2)}(k_{\rho m}b) - H_o^{(2)}(k_{\rho m}\rho)\right]\end{array}\right\}$$
$$+\sum_{l=1}^{N_C}\sum_{n,m}(\nabla\times\hat{z})H_n^{(2)}(k_{\rho m}|\rho-\rho_l|).$$
$$.\cos(k_{zm}z)e^{-jn\phi_l}A_{m,n,l}^M(M_{SRC})$$
$$\phi_l = \angle(\rho-\rho_l), \quad (21)$$

where N_c is the number of cylinders.

A) Treatment of external region

The kernel of integral relevant to external region is separated into two terms, see the expression (18): (*i*) the first term models the unknown magnetic currents flowing on the surface of radiating slots and (*ii*) the second term is relevant to the precomputed PO currents flowing on the inner surface of the radome that takes into account the PO region effects. In fact, the first term of (18) models the condition in which the slots radiate in an infinitely grounded dielectric medium without considering the reflections from the boundary of radome, the second term of (18) models these reflections.

The Green's function of a homogeneous unbounded dielectric region has the following form:

$$\bar{G}_{ext}(r, r') = \left(\bar{I} + \frac{\nabla\nabla}{k^2}\right)\frac{e^{-jk|r-r'|}}{2\pi|r-r'|}, \quad (22)$$

where $k = \omega\sqrt{\mu\varepsilon} = k' - jk''$ is the wave number in the dielectric medium.

In evaluating the first term of $Y_{q,j}^{p,i}(ext)$ in (18) the singular case will occur when $p = q$. In this condition the integral can be evaluated by invoking a suitable change of variables, yielding the following expression:

$$Y_{p,i}^{p,i}(ext) = -j\omega\varepsilon_o\varepsilon_d\frac{1}{\pi k^2}$$
$$.\left[\int_0^{\theta_o}d\theta\int_0^{L_p/\cos\theta}d\rho + \int_{\theta_o}^{\pi/2}d\theta\int_0^{W_i/\sin\theta}d\rho\right]. \quad (23)$$
$$.F_1(\rho, \theta),$$

$$F_1(\rho, \theta) = (W_i - \rho\sin\theta)e^{-jk\rho}$$
$$.\Big[(k^2 - k_p^2)(L_p - \rho\cos\theta)\cos(k_p\rho\cos\theta)$$
$$+\frac{1}{k_p}(k^2 + k_p^2)\sin(k_p\rho\cos\theta)\Big]; \quad (24)$$

with $\theta_o = \tan^{-1}(W_i/L_p)$.

The second term of (18) can be easily computed numerically using Gauss quadrature. (In this case the singularity is not occurring due to the fact that the PO current source, which is following on radome's surface, is always away from the unknown magnetic currents of slots.)

B) Treatment of internal region

The internal region of the geometry consists of two regions of *Ro* and *R1* as shown in Figure1. To evaluate the $Y_{q,j}^{p,i}(\text{int})$, defined in (19), by assuming the corresponding slots in each region, the integral can be decomposed into two parts: the first part takes into account the parallel plates' contribution and the second one coming from the field scattered by the conducting cylinders.

The parallel plates' contribution can be numerically evaluated using Gauss quadrature for two separate modes. However, the singular case that will occur for $p = q$ can be evaluated using the following expression:

$$\hat{v}.\bar{G}_{PPW}(r, r').\hat{v}'|_{\substack{z=z'=h\\ z=z'=2h}}$$
$$= \sum_m\frac{j(1-\frac{\delta_{mo}}{2})}{2k^2h}\left[k^2(\hat{v}.\hat{v}') - \frac{\partial}{\partial v}\frac{\partial}{\partial v'}\right]H_o^{(2)}(k_{\rho m}|\rho-\rho'|), \quad (25)$$

https://doi.org/10.1017/S1759078715000100 Published online by Cambridge University Press

where h is the thickness of the PPW. The singularity $\rho = \rho'$ is easily integrated by adding and subtracting the small argument expression of the Hankel function and using integration by parts [13].

The scattered field contribution is numerically evaluated using H_S^M given in Appendix B.

III. VERIFICATION OF RESULTS

To validate the proposed method, the aforementioned theory is applied to a double layered SIW-based cavity backed slot antenna which has recently been proposed in [7]. This antenna radiates into a thick dielectric slab radome. A comparison between proposed method results and finite element simulations that are carried out using Ansoft's HFSS are presented and discussed.

A) Input impedance and radiation pattern

The double layered SIW cavity backed slot antenna proposed in [7] radiating into a thick dielectric slab radome is considered. The geometry of the antenna-radome system is schematically shown in Fig. 3. Figure 4 shows the SIW cavity backed slot antenna with the corresponding parameters. The SIW antenna structure consists of two main building blocks : the feeding system and the radiating system as shown in Fig. 4. The feeding system and the radiating system are implemented on two different substrate layers.

The vertical walls of structure are realized by rows of metalized posts embedded in a dielectric substrate (RO4003TM) with a relative permittivity of 3.55, a loss tangent of 0.0027 and a thickness of 32 mil. The radiating system includes a main cavity, where the radiating slots are etched on the top

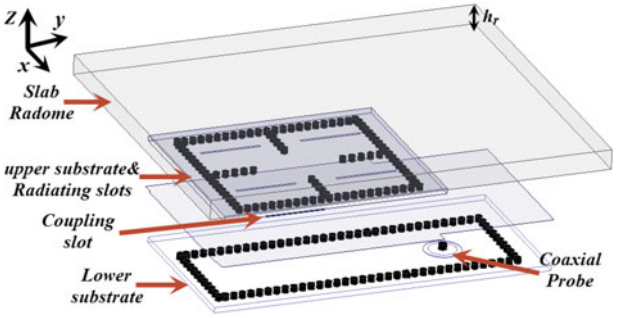

Fig. 3. Representation of the entire antenna with dielectric radome, the dielectric slab thickness is $hr = 2$ cm.

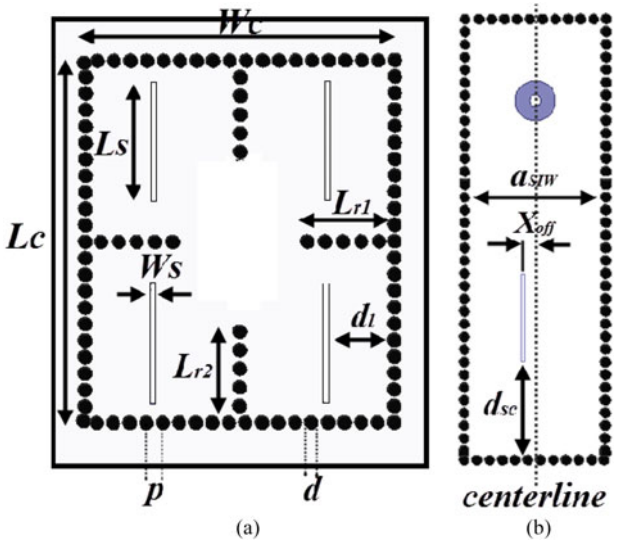

Fig. 4. A schematic view of proposed antenna (a) upper substrate including cavity and radiating slots (b) lower substrate including feeding waveguide and coupling aperture.

Table 1. Antenna parameters and corresponding values.

Parameter	Value (mm)	Parameter	Value (mm)
Lc	27.28	p	1.3
Wc	23.3	d	1
Ls	9	Lr1	6.06
Ws	0.35	Lr2	6.86
dl	4.89	dsc	10.12
a_{SIW}	14.41	Xoff	1.27

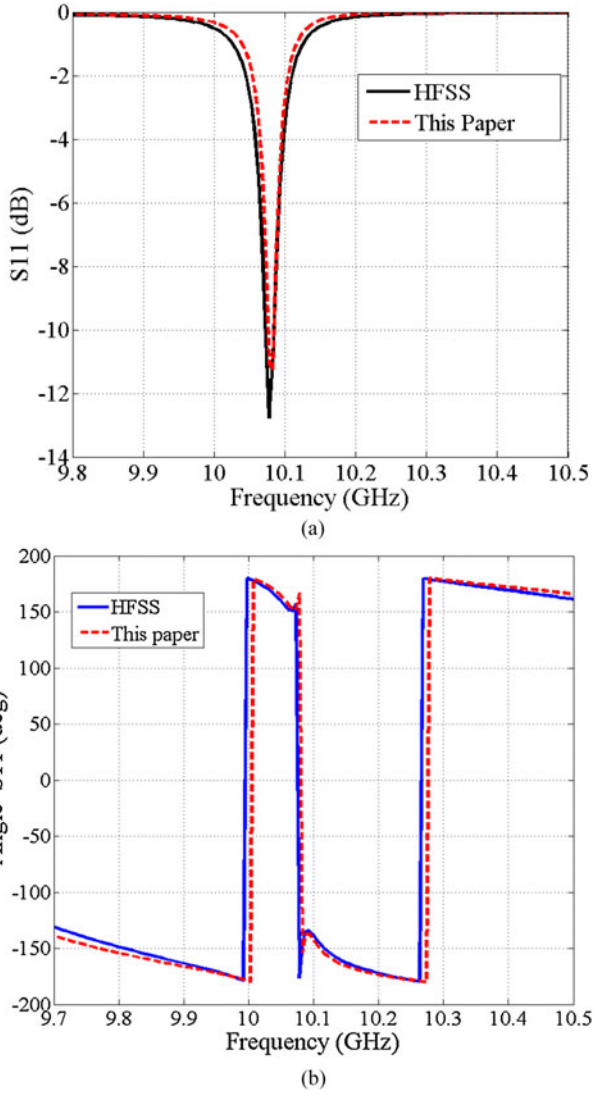

Fig. 5. (a) Magnitude in dB and (b) angle (in degree) of reflection coefficient of the antenna compared with HFSS.

https://doi.org/10.1017/S1759078715000100 Published online by Cambridge University Press

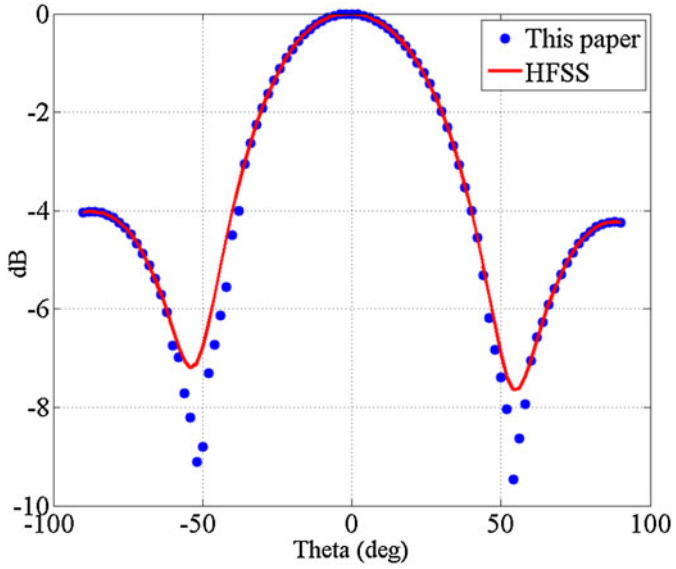

Fig. 6. The total field pattern of the antenna with radome computed by our code and HFSS in y–z plane (the field pattern of the antenna in x–z plane is similar to that in the y–z plane and for the sake of brevity, it is not shown here).

side of metal as shown in Fig. 3. The cavity is divided into four sub-sections with a radiating slot on the top wall of each sub-section. Also, a feeding short circuited SIW waveguide on the rear side of the cavity excites the cavity by a coupling longitudinal slot. In order to connect two layers a coupling longitudinal slot transition located in common face of two SIW blocks is used as shown in Fig. 3. This antenna radiates into a thick dielectric slab radome with constructive parameters $\varepsilon_d = 2.1$ and $\mu_d = 1$: the dielectric slab radome stacked on the top wall of the SIW antenna. A coaxial probe is used to excite the antenna. The antenna parameters and corresponding values are listed in Table 1. Figure 5(a) shows the reflection coefficient of the antenna compared with results obtained from HFSS. The phase of the reflection coefficient of the antenna is also depicted in Fig. 5(b). In Fig. 6 the total field pattern of the antenna with radome is illustrated. In addition, the simulated real and imaginary parts of the input impedance of the antenna, using proposed method and HFSS, are shown in Fig. 7. The results indicate that the proposed method is in very good agreement with those obtained from HFSS.

To show the dielectric radome effects on the input impedance of the antenna, the impedance with and without dielectric slab radome is computed and shown in Fig. 8; from this figure, it can be found that the input impedance of the antenna is strongly altered due to the presence of radome.

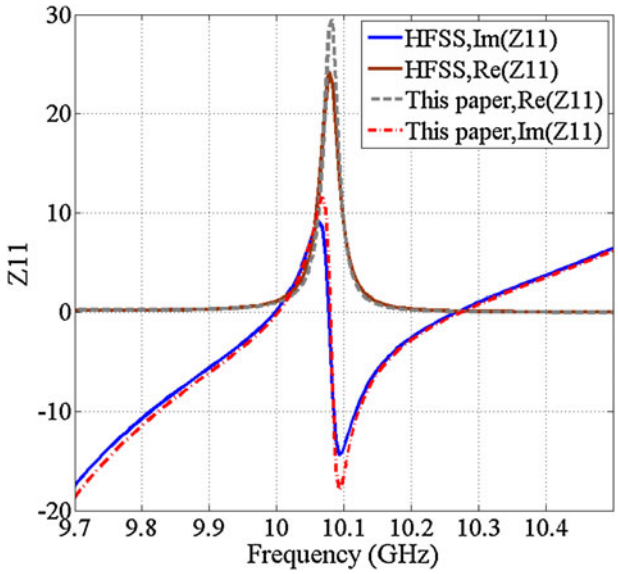

Fig. 7. The simulated real and imaginary parts of the input impedance of the antenna, using our code and HFSS.

B) CPU time and storage requirements

The hybrid method described in the present paper requires three matrices to be filled and inverted: in PO region, a matrix should be filled to compute the PO currents on the radome surface; this matrix dimension depends on the number of points assumed to compute the PO currents; in MoM region, two matrices have been filled, one is necessary to evaluate the field scattered by the metallic via holes and the other one to compute the unknown currents with which the slots have been modeled. The size of matrix in PO region depends on the area that is illuminated by the antenna beam and the number of mesh cells which are assumed to cover this area. By increasing the number of mesh cells, the accuracy of the PO fields, and consequently the CPU processing time and memory requirements, are increased. The simulated results indicate that a $\lambda_g/10 \times /\lambda_g/10$ mesh cell size to cover the illuminated area is enough to ensure the accuracy of the calculated PO fields. In MoM region, the size of the two matrices depends on the number of cylinders *NC*, on the number of slots *Ns*, and on the substrate thickness, which dictates the number of modes *Nz* that will be used.

Tables 2 and 3 report the CPU processing time and storage used in simulating the double layered SIW cavity backed slot antenna with radome, respectively.

By comparing the CPU time and storage, which was used, it can be found that a considerable saving in time and storage capacity is achieved with respect to HFSS, making it possible

https://doi.org/10.1017/S1759078715000100 Published online by Cambridge University Press

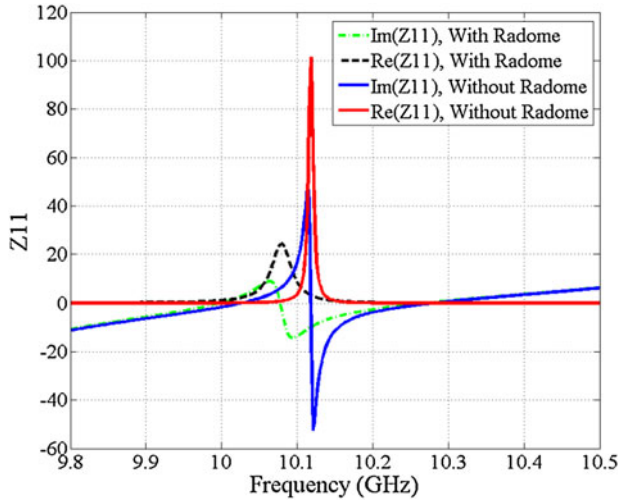

Fig. 8 Impact of radome on the input impedance of the antenna.

Table 2. CPU time (Intel Core i7 3.55 GHz, 16 GB RAM)

Structure type	HFSS CPU time		This paper
	Mesh setup (s)	Frequency point (s)	Frequency point (s)
Antenna without radome	74	65	3
Antenna with radome	82	77	5

Table 3. Memory requirement

Structure type	HFSS (GB)	This paper (GB)
Antenna without radome	3.01	0.12
Antenna with radome	5.79	0.2

to simulate larger structure with limited computing resources with acceptable accuracy. The advantage of the proposed method is more bolder when a complex, multilayered SIW-based antenna radiated into a large (very thick) dielectric radome, is considered. In this case HFSS may be unable to simulate the structure with the computer resources available or the simulation will be more time consuming.

V. CONCLUSION

In this paper, a fast and efficient full-wave method based on a hybrid MoM–PO implementation for the rigorous study of complex, multilayered SIW-based antenna structures, when a dielectric slab radome is located in front of the antenna, have been presented. In addition, the reverse coupling from the radome to the antenna is assumed in spite of pervious works done on the modeling of radomes. The results of the analysis of a double-layered SIW cavity backed slot antenna radiating into a dielectric slab radome using our code were compared to the ones obtained by the commercial FEM-based solver HFSS. The results show a very good agreement, indicating the validity of our approach with an extreme reduction of computational time and storage capacity. The fast calculation feature as well as accuracy of our code makes it suitable for the implementation of optimization techniques for a complex multilayered SIW structure with or without the radome shell.

REFERENCES

[1] Hirokawa, J.; Ando, M.: Single-layer feed waveguide consisting of posts for plane TEM wave excitation in parallel plates. IEEE Trans. Antennas Propag., **46** (2) (1998), 625–630.

[2] Jin, H.; Wen, G.: A novel four-way Ka-band spatial power combiner based on HMSIW. IEEE Microw. Wirel. Compon. Lett., **18** (8) (2008), 515–517.

[3] Chen, J.-X.; Hao, Z.-C.; Li, H.; Wu, K.: Development of a low cost microwave mixer using a broadband substrate integrated waveguide (SIW) coupler. IEEE Microw. Wirel. Compon. Lett., **16** (2) (2006), 84–86.

[4] Cassivi, Y.; Wu, K.: Low cost microwave oscillator using substrate integrated waveguide cavity. IEEE Microw. Wirel. Compon. Lett., **13** (2) (2003), 48–50.

[5] Abdolhamidi, M.; Shahabadi, M.: X-band substrate integrated waveguide amplifier. IEEE Microw. Wirel. Compon. Lett., **18** (12) (2008), 815–817.

[6] Yan, L.; Hong, W.; Hua, G.; Chen, J.; Wu, K.; Cui, T.J.: Simulation and experiment on SIW slot array antennas. IEEE Microw. Wirel. Compon. Lett., **14** (9) (2004), 446–448.

[7] Bayderkhani, R.; Forooraghi, K.; Abbasi-arand, B.: Gain intensified slot antennas backed by SIW cavity using high order cavity resonance. Int. J. Microw. Wirel. Tech., (2014), doi:10.1017/S1759078714001202.

[8] Kishihara, M.; Yamane, K.; Ohta, I.: Analysis of post-wall waveguide by H-plane planar circuit approach. IEEE MTT-S Int. Microwave Symp., Honolulu, HA, 2007.

[9] Deslandes, D.; Perregrini, L.; Arcioni, P.; Bressan, M.; Wu, K.; Conciauro, G.: Dispersion characteristics of substrate integrated rectangular waveguide. IEEE Microw. Wirel. Compon. Lett., **12** (2002), 333–335.

[10] Abaei, E.; Mehrshahi, E.; Amendola, G.; Arnieri, E.; Shamsafar, A.: Two dimensional multi-port method for analysis of propagation characteristics of substrate integrated waveguide. Prog. Electromagn. Res. C, **29** (2012), 261–273.

[11] Arnieri, E.; Amendola, G.: Analysis of substrate integrated waveguide structures based on the parallel-plate waveguide Green's function. IEEE Trans. Microw. Theory Tech., **56** (2008), 1615–1623.

[12] Amendola, G.; Arnieri, E.; Boccla, E.: Analysis of lossy SIW structures based on the parallel plates waveguide Green's function. Prog. Electromagn. Res. C, **33** (2012), 157–169.

[13] Arnieri, E.; Amendola, G.: Method of moments analysis of slotted substrate integrated waveguide arrays. IEEE Trans. Antennas Propag., **59** (4) (2011), 1148–1154.

[14] Casaletti, M.; Valerio, G.; Seljan, J.; Ettorre, M.; Sauleau, R.: A full-wave hybrid method for the analysis of multilayered SIW-based antennas. IEEE Trans. Antennas Propag., **61** (11) (2013), 5575–5588.

[15] Gao, X.J.; Felsen, L.B.: Complex ray analysis of beam transmission through two dimensional radomes. IEEE Trans. Antennas Propag., **33** (9) (1985), 963–975.

[16] Abdel moneum, M.A.; Shen, Z.X.; Volakis, J.L.; Graham, O.: Hybrid PO-MoM analysis of large axi-symetrical radomes. IEEE Trans. Antennas Propag., **49** (12) (2001), 1657–1666.

https://doi.org/10.1017/S1759078715000100 Published online by Cambridge University Press

[17] Meng, H.F.; Dou, W.B.: Analysis of radome using aperture integration-surface integration method with modified transmission coefficient. J. Infrared Millim. Terahertz Waves, **30** (2) (2009), 199–210.

[18] Meng, H.F.; Dou, W.B.: Hybrid IPO-BI-FEM for the analysis of 2D large radome with complex structure. Microw. Opt. Technol. Letter, **51** (5) (2009), 1348–1353.

[19] Harrington, R.F.: Time-Harmonic Electromagnetic Fields, Wiley-IEEE Press, New York, 2001.

[20] Ishimaru, A.: Electromagnetic Wave Propagation, Radiation, and Scattering, Prentice-Hall, Englewood Cliffs, 1991.

Reza Bayderkhani was born on February 10, 1985, in Tehran, Iran. He received the B.Sc. degree in electrical engineering, in 2007, and the M.Sc. degree (*with honors*) in communication engineering, in 2010, both from the Shahed University, Tehran, Iran. He is currently working towards the Ph.D. degree in electrical engineering (communication, field & wave) at the Tarbiat Modares University(TMU). His research interests include computational electromagnetic, planar antenna structures and arrays, and SIW structures.

Keyvan Forooraghi was born in Tehran, Iran. He received the Msc., Technology Licentiate and PhD from Chalmers University of Technology, Gothenburg, Sweden, in 1983, 1988 and 1991 respectively, all in electrical engineering. He was a researcher at the department of network theory during 1992-1993. He joined the department of electrical engineering at Tarbiat Modares University (TMU) in 1993 where he currently is a professor and lectures on electromagnetic, antenna theory and design, and microwave circuits. His research interests include computational electromagnetic, waveguide slot antenna design and microstrip antennas.

Emilio Arnieri was born in Cosenza, Italy, in 1977. He received the degree (with honors) in information technology engineering from the University of Calabria, Rende, Italy, in 2003 and the Ph.D. degree in electronic engineering from the University "Mediterranea" of Reggio Calabria, in 2007. Currently, he is an Assistant Professor with the Dept. of Informatics, Modeling, Electronics and System Engineering(DIMES), University of Calabria (Italy). His main research activities concern the development of dual band antennas and millimeter-wave components, development of numerical methods for the electromagnetic modeling of microwave and millimeter-wave circuits (substrate integrated circuits, slotted substrate integrated waveguide arrays, and substrate integrated waveguide resonators).

Bijan Abbasi Arand received the B.Sc. from the Shiraz University, Shiraz, Iran in 1995 and the M.S. and Ph.D. degrees in Telecommunication engineering from Tarbiat Modares University, Tehran, Iran in 1997 and 2003, respectively.

From 2003 to 2005, He was a researcher of electromagnetic propagation department in Iran Telecommunication Research Center (ITRC).

In 2005, he joined the Satellite communication laboratory of Tarbiat Modares as a Postdoctoral researcher. Since 2010, he is assistant professor in faculty of Electrical and Computer engineering of Tarbiat Modares. He has more than 35 papers and publications in journal and conferences.

APPENDIX A

The dyadic Green's function of the parallel plate waveguide has the following form [11]:

$$\begin{aligned}\bar{G}_{PPW}(r,r') = &-\frac{1}{k^2}\hat{z}\hat{z}\delta(r-r') - j\sum_m\left(1-\frac{\delta_{m0}}{2}\right)\frac{1}{2k_{\rho m}^2 h}\\ &[(\nabla\times\hat{z})(\nabla'\times\hat{z})H_0^{(2)}(k_{\rho m}|\rho-\rho'|)f_c(k_{zm},z,z')\\ &+\frac{1}{k^2}(\nabla\times\nabla\times\hat{z})(\nabla'\times\nabla'\times\hat{z})H_0^{(2)}\\ &.(k_{\rho m}|\rho-\rho'|)f_s(k_{zm},z,z')],\end{aligned} \tag{A.1}$$

with $k=\omega\sqrt{\mu\varepsilon_0\varepsilon}$, $k_{zm}=m\pi/h$, $k_{\rho m}=\sqrt{k^2-k_{zm}^2}$ and

$$\delta_{m0}=\begin{cases}1 & for \quad m=0\\ 0 & for \quad m\neq 0\end{cases}, \tag{A.2}$$

$$f_{c,s}=\begin{pmatrix}\cos(k_{zm}z)\cos(k_{zm}z')\\ \sin(k_{zm}z)\sin(k_{zm}z')\end{pmatrix}, \tag{A.3}$$

where k is the wave number, k_{zm} is the wave number in z direction and $k_{\rho m}$ is the radial wave number.

APPENDIX B

H_S^M is expressed as the series of outgoing cylindrical waves cantered on the metallic cylinders and it has the following form:

$$\begin{aligned}H_S^M(r) = &\sum_{l,n,m}\nabla\times\begin{bmatrix}H_n^{(2)}(k_{\rho m}|\rho-\rho_l|)e^{-jn\varphi}\\ .\cos k_{zm}(h-z)\hat{z}\end{bmatrix}A_{m,n,l}^M(M)\\ &+\sum_{l,n,m}\frac{1}{k}\nabla\times\nabla\times\begin{bmatrix}H_n^{(2)}(k_{\rho m}|\rho-\rho_l|)e^{-jn\varphi}\\ .\sin k_{zm}(h-z)\hat{z}\end{bmatrix}A_{m,n,l}^N(M)\\ &\varphi=\angle(\rho-\rho_l).\end{aligned} \tag{B.1}$$

In (B.1), m spans the number of vertical modes, and spans the number of radial modes, l spans the number of cylinders, and ρ_l is the position of the center of the cylinder l. Enforcing the boundary conditions on the metallic posts yield the scattering amplitudes, $A_{m,n,l}^M$ (TM mode) and $A_{m,n,l}^N$ (TE mode) [11].

https://doi.org/10.1017/S1759078715000100 Published online by Cambridge University Press